ACS APPLIED MATERIALS & INTERFACES

Research Article

www.acsami.org

# Blending Homopolymers for Controlling the Morphology Transitions of Block Copolymer Nanorods Confined in Cylindrical Nanopores

Ming-Hsiang Cheng, Yu-Chen Hsu, Chun-Wei Chang, Hao-Wen Ko, Pei-Yun Chung, and Jiun-Tai Chen*

Department of Applied Chemistry, National Chiao Tung University, Hsinchu, Taiwan 30010

Supporting Information

**ABSTRACT:** The microphase separation of block copolymers in confined geometries has been widely investigated over the last few decades. The controllability and versatility of the confinement-induced morphologies, however, are still difficult to be achieved because of the limited experimental parameters in the process of fabricating the confined nanostructures. In this work, we study the morphology transitions of lamellae-forming polystyrene-*block*-polydimethylsiloxane (PS-*b*-PDMS) nanorods confined in the nanopores of anodic aluminum oxide (AAO) templates. The nanorods are formed by solvent-assisted template wetting, and the morphologies are compared to those in the bulk state. By blending PS-*b*-PDMS with homopolystyrene (hPS), the morphologies of the nanorods can be controlled because of the changes of the effective volume fractions. Special morphology transitions from concentric lamellar morphology, to multihelical morphology, and finally to spherical-like morphology are observed by increasing the weight ratios of hPS. hPS with different molecular weights is also applied to investigate the effect of hPS on the morphologies of the PS-*b*-PDMS/hPS blend nanostructures. The unusual morphologies are further confirmed by a selective removal process, which also generates nanochannels for possible refilling with functional materials.

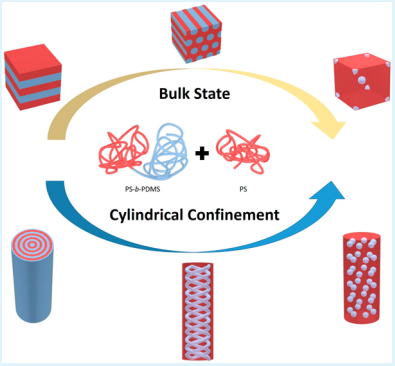


**KEYWORDS:** *block copolymer/homopolymer blends, self-assembly, template, solvent annealing, nanoporous materials*

## INTRODUCTION

Block copolymers (BCPs), which can self-assemble into highly ordered arrays of microphase-separated nanostructures, have been intensively investigated over the last few decades.[1,2] Depending on the molecular architectures and constituents of BCPs, various morphologies including lamellae, gyroids, cylinders, and spheres can be obtained.[3−5] These microphase-separated polymer structures can be applied to different applications such as photovoltaics, sensors, nanolithography, and optics.[6−9] If one of the polymer segments with less resistance to specific irradiation or solvents can be etched selectively, polymer materials with ordered nanoporous arrays can be generated.[10−12]

In recent years, the investigations of block copolymers in confined geometries, especially in cylindrical nanopores, have aroused more interest.[13−15] For block copolymers confined in cylindrical nanopores, the curvature and incommensurability between the pore sizes and the repeating periods of the block copolymers cause the formation of unusual morphologies, which have not been observed in the bulk state.[15,16] Templates containing cylindrical nanopores are usually used to confine block copolymers. Among various porous templates, the anodic aluminum oxide (AAO) template is one of the most commonly used templates because of the well-controlled dimensions such as the pore lengths, pore to pore distances, and pore diameters, which can be controlled by altering different processing conditions.[17,18]

Using AAO templates, homopolymers or block copolymers have been introduced into the nanopores using different template wetting methods.[19] Four template wetting methods are commonly used for the infiltration of polymers into the nanopores of AAO templates, including the solution wetting method, the melt wetting method, the microwave-annealing-induced nanowetting (MAIN) method, and the solvent-annealing-induced nanowetting in template (SAINT) method. In the solution wetting method, polymers can be infiltrated into the nanopores of the templates via capillary force by immersing the template in the polymer solutions.[20,21] In the melt wetting method, polymer films or powders can be introduced into the nanopores by heating the polymers above the glass transition temperatures ($T_g$) or the melting temperatures ($T_m$); the wetting mechanisms are controlled by changing the annealing conditions.[16,22,23] Comparing with the melt wetting method, polymers can be infiltrated into the nanopores in a shorter processing time by the microwave-annealing-induced nanowetting (MAIN) method.[24] The fourth template wetting method is the solvent-annealing-induced nanowetting in templates (SAINT) method; polymers can be introduced into the nanopores of the templates by annealing the samples in the presence of solvent vapors.[25,26]

**Received:** April 18, 2017
**Accepted:** May 30, 2017
**Published:** May 30, 2017

ACS Publications © 2017 American Chemical Society



DOI: 10.1021/acsami.7b05415
*ACS Appl. Mater. Interfaces* 2017, 9, 21010−21016

For block copolymers, the polymer chains can be introduced into the nanopores using the above methods. For example, Russell et al. used the solution wetting method to study the morphologies of polystyrene-*block*-poly(ethylene oxide) (PS-*b*-PEO) nanotubes confined in the nanopores of the AAO templates.[27] After the PS-*b*-PEO nanotubes were dipped in mixed solvents of water/methanol, the PEO domains can be selectively swollen, leaving nanopores on the surfaces of the nanotubes. For the melt wetting method, Russell et al. studied the morphologies of polystyrene-*block*-polybutadiene (PS-*b*-PBD) confined in the nanopores of AAO templates.[16,28] The relationship between the morphologies of the block copolymers and the pore sizes of the AAO templates was investigated. Lamellar, cylindrical, and spherical forming PS-*b*-PBD block copolymers were used in their works, and special morphologies such as toroids or double helices were observed. Steinhart et al. also used the melt wetting method to investigate the morphologies of polystyrene-*block*-poly(methyl methacrylate) (PS-*b*-PMMA) confined in the nanopores of AAO templates.[29,30] After the PMMA domains were selectively removed by UV irradiation and acetic acid washing, mesoporous PS nanorods were obtained. For the SAINT method, we previously studied the morphologies of polystyrene-*block*-polydimethylsiloxane (PS-*b*-PDMS) block copolymer confined in the nanopores of AAO templates using different annealing solvent vapors.[26]

Although block copolymer nanostructures confined in cylindrical nanopores can be prepared by different template wetting methods, the control over the confinement-induced morphologies is still limited to a few parameters, such as the pore sizes of the nanopores, the volume fractions of the polymer segments, and the surface and interfacial tensions of the materials.[14,28,29,31]

To overcome the limitations of the fewer experimental parameters and extend the possibilities of the confinement-induced morphologies, here we propose a facile and reliable concept by blending BCPs with homopolymers for the fabrication of confined nanostructures. Lamellae-forming polystyrene-*block*-polydimethylsiloxane (PS-*b*-PDMS) copolymers blended with different amounts of homopolystyrene (hPS) are infiltrated into the nanopores of AAO templates using the SAINT method. The microphase separation of the blend nanorods is compared to those in the bulk state. The effective volume fractions of PS and PDMS domains can be changed by adding different amounts of hPS, resulting in the formation of nanorods with different morphologies. Morphology transitions from concentric lamellar morphology, to multihelical morphology, and finally to spherical-like morphology can be observed by increasing the weight ratios of hPS. hPS with different molecular weights are also used to study the effect of hPS on the morphologies of the PS-*b*-PDMS/hPS blend nanostructures. The morphologies can be further determined by a selective removal process using HF solution to etch the PDMS domains selectively. This work demonstrates that blending block copolymers with homopolymers is a powerful approach to control the morphologies of block copolymer nanostructures confined in cylindrical nanopores.

## EXPERIMENTAL SECTION

**Materials.** Lamellae-forming polystyrene-*block*-polydimethylsiloxane (PS-*b*-PDMS, 22-*b*-21 kg/mol) with a polydispersity index (PDI) of 1.08 and homopolystyrene (hPS) were obtained from Polymer Source. The PDIs for the hPS ($M_n$: 4.7, 24, and 820 kg/mol) are 1.14, 1.05, and 1.14, respectively. Toluene was purchased from Tedia. Deionized water was obtained from the Milli-Q system. Ammonium hydroxide ($NH_4OH$) was purchased from Merck. Ethanol, isopropyl alcohol, and acetone were acquired from Echo Chemical. Hydrogen fluoride (HF) was purchased from Union Chemicals. Four-inch Si (100) wafers were obtained from Guv Team International Co., Ltd. Polycarbonate filters (VCTP, pore size ~0.1 $\mu$m) were purchased from Millipore. Anodic aluminum oxide (AAO) templates (pore diameter ~150−400 nm, thickness ~60 $\mu$m) were purchased from Whatman.

**Fabrication of PS-*b*-PDMS/hPS in Bulk, Thin-Film, and Confinement States.** For the fabrication of PS-*b*-PDMS/hPS blends in the bulk state, PS-*b*-PDMS/hPS blend solutions with different weight ratios were first prepared by dissolving PS-*b*-PDMS and hPS in toluene and stirred for 24 h. After the complete dissolution of the polymers, toluene was slowly evaporated at room temperature. The residual solvents were then removed by placing the sample bottles in a 60 °C oven for 3 days, and PS-*b*-PDMS/hPS blend powders can be obtained.

For the fabrication of PS-*b*-PDMS/hPS blend thin films, PS-*b*-PDMS/hPS blend solutions with various weight ratios were prepared by dissolving PS-*b*-PDMS and hPS in toluene and stirred for 24 h. The samples were spin coated on silicon wafers (1.3 cm × 1.3 cm) at 2000 rpm for 40 s. After the spin-coating process, the samples were vacuumed to remove the residual solvents. A solvent vapor annealing process was also applied. As-spun PS-*b*-PDMS/hPS thin films with different weight ratios were placed into a glass chamber with an open bottle of the annealing solvent (toluene). A parafilm was used to seal the annealing chamber to prevent the annealing solvents from leaking. The solvent vapor annealing process was conducted at a constant temperature of 30 °C for 24 h. After the solvent vapor annealing process, the annealed PS-*b*-PDMS/hPS thin films were taken out from the glass chamber and dried using a vacuum pump.

For the fabrication of PS-*b*-PDMS/hPS blend nanostructures confined in the AAO nanopores, PS-*b*-PDMS/hPS blend solutions with different weight ratios were first prepared by dissolving PS-*b*-PDMS and hPS in toluene and stirred for 24 h. The polymer blend solutions (50 $\mu$L) were then dropped onto silicon wafers (1.3 cm × 1.3 cm). After toluene was slowly evaporated at room temperature, the residual solvents were removed using a vacuum pump, and PS-*b*-PDMS/hPS blend films can be obtained. Later, AAO templates were carefully placed on the top of the polymer films. The samples were then transferred into a solvent annealing chamber, a glass bottle which contained an open bottle of the annealing solvent (toluene). The solvent vapor annealing process was conducted at a constant temperature of 30 °C for 24 h, and a parafilm was used to seal the glass chamber for avoiding the leakage of the solvent vapors. After the solvent vapor annealing process, the samples were taken out from the glass chamber and dried using a vacuum pump. The AAO templates were later dissolved selectively by using 5 wt % $NH_4OH$ solutions. Finally, the samples were washed with deionized water several times and filtered with polycarbonate membranes.

For the selective removal process, a 48 wt % HF solution was dropped onto the samples to dissolve the PDMS domains selectively. The selective removal step was conducted for 8 h, and the samples were further dried using a vacuum pump.

**Structure Analysis and Characterization.** Small-angle X-ray scattering (SAXS) experiments were conducted to examine the microphase separation of $PS_{22k}$-*b*-$PDMS_{21k}$/hPS blends in the bulk state using a 10 keV photon beam with a wavelength of 1.24 Å and a diameter of 0.5 mm at the beamline BL23A of the National Synchrotron Radiations Research Center (NSRRC). Samples were sealed between two thin Kapton windows and measured at ambient conditions. An atomic force microscope (AFM, Innova) with a soft tapping mode was applied to examine the surface topography and the phase separation behavior of the block copolymer thin films. Before the AFM measurements, the samples were vacuumed to remove the residual solvents. A scanning electron microscope (SEM, JEOL JSM-7401) at an acceleration voltage of 5 kV was used to examine the surface morphologies of the $PS_{22k}$-*b*-$PDMS_{21k}$/hPS blend nanostructures confined in the AAO nanopores. Before the SEM measurements,


DOI: 10.1021/acsami.7b05415
ACS Appl. Mater. Interfaces 2017, 9, 21010−21016

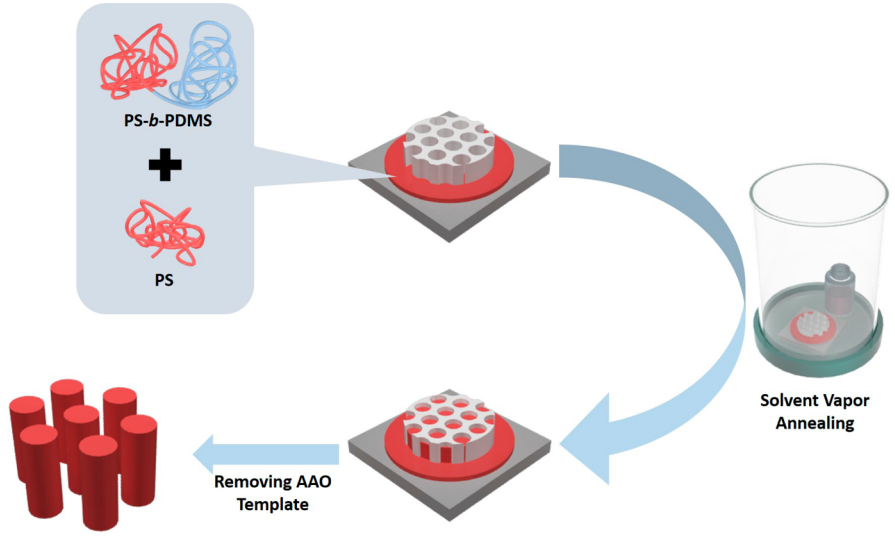


**Figure 1.** Schematic illustration for fabricating $PS_{22k}$-*b*-$PDMS_{21k}$/hPS blend nanostructures. The sample covered with an AAO template is annealed in a glass chamber that contains an open bottle of toluene, the annealing solvent. After the solvent vapor annealing process, the AAO template is etched selectively by a $NH_4OH$ solution, and polymer nanostructures can be obtained.

the samples were dried using a vacuum pump and coated with 4 nm of platinum. A transmission electron microscope (TEM, JEOL JEM-2100) with an acceleration voltage of 200 kV was also used to characterize the internal morphologies of the $PS_{22k}$-*b*-$PDMS_{21k}$/hPS blend nanostructures. Before the TEM measurements, the samples were placed onto copper grids coated with Formvar or carbon and dried by a vacuum pump.

## RESULTS AND DISCUSSION

Figure 1 shows the experimental process for the fabrication of $PS_{22k}$-*b*-$PDMS_{21k}$/hPS blend nanostructures confined in the nanopores of AAO templates using the SAINT method. First, $PS_{22k}$-*b*-$PDMS_{21k}$/hPS solutions with different weight ratios are dropped onto silicon wafers and dried using a vacuum pump. The dried $PS_{22k}$-*b*-$PDMS_{21k}$/hPS blend films are then covered with AAO templates. The samples are later transferred into a sealed glass chamber and annealed in toluene vapors at 30 °C for 24 h. After the solvent vapor annealing process, the samples are taken out from the annealing chamber and dried using a vacuum pump. By selectively dissolving the AAO templates using $NH_4OH$(aq), $PS_{22k}$-*b*-$PDMS_{21k}$/hPS blend nanostructures can be obtained. The PDMS domains in the nanostructures can also be selectively etched using the HF solution, resulting in the formation of porous PS nanostructures.

For $PS_{22k}$-*b*-$PDMS_{21k}$/$hPS_{24k}$ blends with different weight ratios, SAXS measurements are first conducted to characterize the microphase separation behavior in the bulk state. As the weight ratio of the $hPS_{24k}$ increases, the morphology changes from lamellar morphology to hexagonal-packed cylindrical morphology, as shown in Figure 2. The relative $q$ values of 1:2:3:4 indicate the formation of lamellar morphology for $PS_{22k}$-*b*-$PDMS_{21k}$/$hPS_{24k}$ blends with the weight ratio of $hPS_{24k}$ lower than 0.25, as shown in curves A–C in Figure 2; the relative $q$ values of $1:2:\sqrt{7}$ indicate the formation of hexagonal-packed cylindrical morphology for $PS_{22k}$-*b*-$PDMS_{21k}$/$hPS_{24k}$ blends with the weight ratio of $hPS_{24k}$ equal to 0.5, as shown in curve D in Figure 2. As the weight ratio of $hPS_{24k}$ further increases to 1, the morphology is difficult to identify from the SAXS data, as shown in curve E in Figure 2.

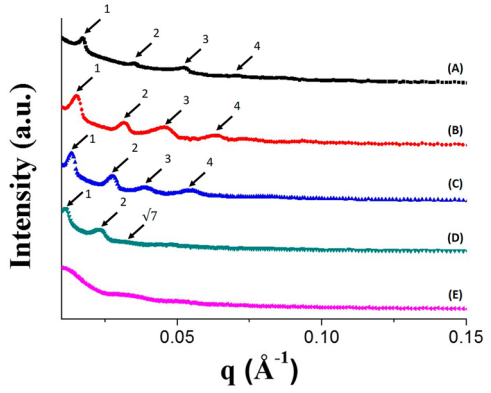


**Figure 2.** SAXS data for the $PS_{22k}$-*b*-$PDMS_{21k}$/$hPS_{24k}$ blends in the bulk state with different weight ratios ($PS_{22k}$-*b*-$PDMS_{21k}$/$hPS_{24k}$): (A) 1/0, (B) 1/0.1, (C) 1/0.25, (D) 1/0.5, and (E) 1/1.

For the morphology transitions of $PS_{22k}$-*b*-$PDMS_{21k}$/$hPS_{24k}$ in the thin-film state, AFM characterization is conducted to determine the microphase separation behavior, as shown in Figure 3. Figure 3A–E shows the AFM phase images of the as-

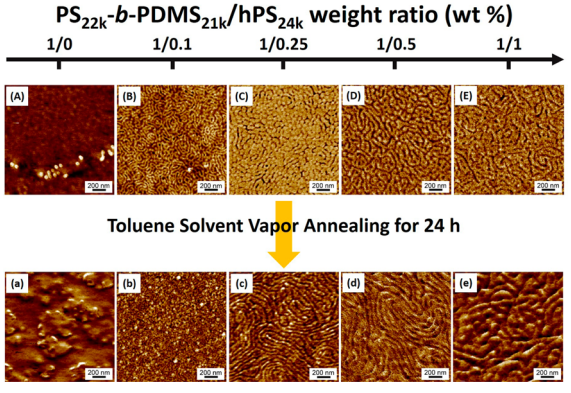


**Figure 3.** AFM phase images of the as-spun and toluene-vapor-annealed $PS_{22k}$-*b*-$PDMS_{21k}$/$hPS_{24k}$ thin films: (A and a) 1/0, (B and b) 1/0.1, (C and c) 1/0.25, (D and d) 1/0.5, and (E and e) 1/1.



DOI: 10.1021/acsami.7b05415
ACS Appl. Mater. Interfaces 2017, 9, 21010–21016

spun $PS_{22k}$-*b*-$PDMS_{21k}$/$hPS_{24k}$ thin films. Without the addition of $hPS_{24k}$, $PS_{22k}$-*b*-$PDMS_{21k}$ thin film shows lamellar morphology parallel to the substrate, as shown in Figure 3A. With the addition of $hPS_{24k}$, microphase separation of the $PS_{22k}$-*b*-$PDMS_{21k}$/$hPS_{24k}$ thin films can be observed (Figure 3B–E), in which the brighter regions indicate the PS segments, while the darker regions indicate the PDMS segments. As the weight ratio of $hPS_{24k}$ increases, the darker regions (the PDMS segments) decrease, indicating the higher ratios of the PS domains in the $PS_{22k}$-*b*-$PDMS_{21k}$/$hPS_{24k}$ blends.

The $PS_{22k}$-*b*-$PDMS_{21k}$/$hPS_{24k}$ thin films are also annealed in toluene vapors, as shown in Figure 3a–e. The roughness in Figure 3a is probably due to the differences in the height of the lamellar-forming structures with different numbers of repeating periods. After the solvent vapor annealing process, the morphology of the $PS_{22k}$-*b*-$PDMS_{21k}$/$hPS_{24k}$ thin film with the blending ratio of 1/0.1 changes to parallel lamellar morphology (Figure 3b). The more distorted morphologies of $PS_{22k}$-*b*-$PDMS_{21k}$/$hPS_{24k}$ thin films with the blending ratio of 1/1 before and after annealing, as shown in Figure 3E and 3e, also agree with the SAXS results (Figure 2E), in which the characteristic peak is absent as the weight ratio of $hPS_{24k}$ further increases to 1.

By infiltrating $PS_{22k}$-*b*-$PDMS_{21k}$/$hPS_{24k}$ blends into the AAO nanopores using the SAINT method in toluene vapors, various $PS_{22k}$-*b*-$PDMS_{21k}$/$hPS_{24k}$ blend nanostructures can be obtained. SEM and TEM measurements are applied to determine the surface and internal morphologies of the $PS_{22k}$-*b*-$PDMS_{21k}$/$hPS_{24k}$ blend nanostructures, as shown in Figure 4. Figure 4A–E shows the SEM images of the $PS_{22k}$-*b*-$PDMS_{21k}$/$hPS_{24k}$ blend nanostructures with different weight ratios; similar smooth morphologies are observed because of the formation of the PDMS wetting layer on the pore walls of the AAO templates.

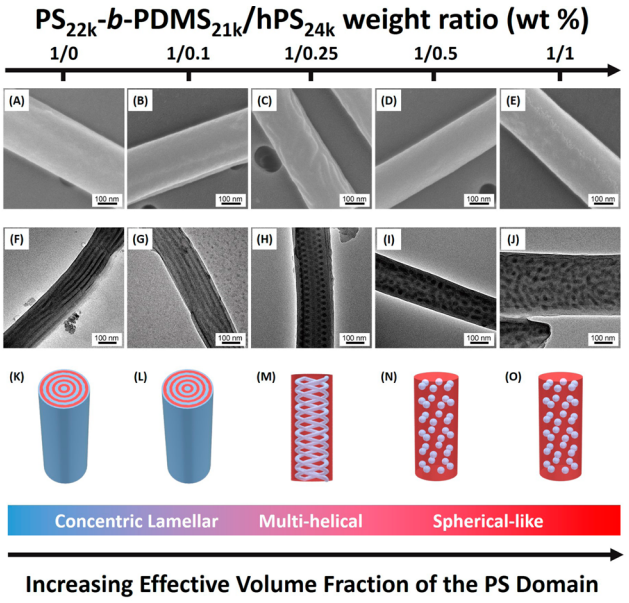


**Figure 4.** SEM images (A–E), TEM images (F–J), and corresponding graphical illustrations (K–O) for the $PS_{22k}$-*b*-$PDMS_{21k}$/$hPS_{24k}$ blend nanostructures with different weight ratios ($PS_{22k}$-*b*-$PDMS_{21k}$/$hPS_{24k}$): (A, F, and K) 1/0, (B, G, and L) 1/0.1, (C, H, and M) 1/0.25, (D, I, and N) 1/0.5, and (E, J, and O) 1/1.

The internal morphologies of the nanostructures can be determined from the TEM images, in which the darker domains represent PDMS because of the higher electron density of the PDMS block than that of the PS block. From TEM characterization, it can be observed that the outermost layer is the PDMS domain because of the stronger interactions between PDMS and AAO walls than those between PS and AAO walls.

By controlling the blending ratios of block copolymer/homopolymer, the transitions of internal morphologies can be obtained, as shown in the TEM images (Figure 4F–J) and corresponding graphical illustrations (Figure 4K–O). Without the addition of $hPS_{24k}$, concentric lamellar morphology is observed, similar to our previous results using lamellae-forming $PS_{22k}$-*b*-$PDMS_{21k}$,[32] as shown in Figure 4F and 4K. When the weight ratio of $PS_{22k}$-*b*-$PDMS_{21k}$/$hPS_{24k}$ changes to 1/0.1, the effective volume fraction of the PS domains increases but is not enough to induce the morphology transition; therefore, concentric lamellar morphology is still maintained, as shown in Figure 4G and 4L. As the weight ratio of $PS_{22k}$-*b*-$PDMS_{21k}$/$hPS_{24k}$ further changes to 1/0.25, the increased effective volume fraction of the PS domains causes the morphology transition from concentric lamellar morphology to multihelical morphology, as displayed in Figure 4H and 4M. The determination of the multihelical structures shown in Figure 4H and the pitches and diameters of the PDMS strands are presented in Figure S1. At the weight ratios of 1/0.5 and 1/1, the effective volume fractions of the PS domains become even larger, and spherical-like morphology is observed, as shown in Figure 4I, 4J, 4N, and 4O; the diameter of PDMS nanospheres in the spherical-like structures is measured to be ~26 nm. By blending $PS_{22k}$-*b*-$PDMS_{21k}$ with $hPS_{24k}$, the morphologies of the polymer nanostructures can be adjusted from concentric lamellar morphology, to multihelical morphology, and finally to spherical-like morphology; such unique morphologies, especially the multihelical morphology, are different from those in the bulk state. The nonperiodic structure in the spherical-like morphologies is mainly due to the overblending of homopolystyrene and the ratio between the molecular weight of the homopolymers and that of the corresponding block copolymer segments, which may lead to the macrophase separation between the block copolymers and the homopolymers.[33,34]

To further investigate the effect of blending hPS on the morphologies of the PS-*b*-PDMS/hPS nanorods, polystyrenes with different molecular weights are used. Hashimoto et al. investigated that the microphase separation behavior of block copolymer/homopolymer blends in the bulk state can be controlled by the blending ratios of homopolymers and the ratio $r_M$ ($r_M = M_H/M_C$) between the molecular weight of the homopolymers ($M_H$) and the identical polymer segments ($M_C$) in the block copolymers.[33,34] They concluded that the homopolymer segments can diffuse into the corresponding block copolymer segments and "wet" the block copolymer segments, and "wet brush" occurs, when the molecular weight of homopolymers is smaller than that of the corresponding block copolymer segments ($r_M < 1$). When the molecular weight of homopolymers is much larger than that of the corresponding block copolymer segments ($r_M \gg 1$), "dry brush" occurs, and the macrophase separation between block copolymer and homopolymer exists. When $r_M$ is near unity, the intermediate state between the "wet brush" and "dry brush" occurs.

In this work, we use polystyrenes with different molecular weights to change the $r_M$ values. In addition to $hPS_{24k}$ ($r_M \sim 1$), $PS_{22k}$-*b*-$PDMS_{21k}$ are also blended with $hPS_{4.7k}$ ($r_M < 1$) and


DOI: 10.1021/acsami.7b05415
ACS Appl. Mater. Interfaces 2017, 9, 21010–21016

$hPS_{820k}$ ($r_M \gg 1$). The TEM images of the $PS_{22k}$-*b*-$PDMS_{21k}$/hPS nanostructures with different molecular weights of hPS are summarized in Figure 5. For $PS_{22k}$-*b*-$PDMS_{21k}$/$hPS_{24k}$ ($r_M \sim 1$),

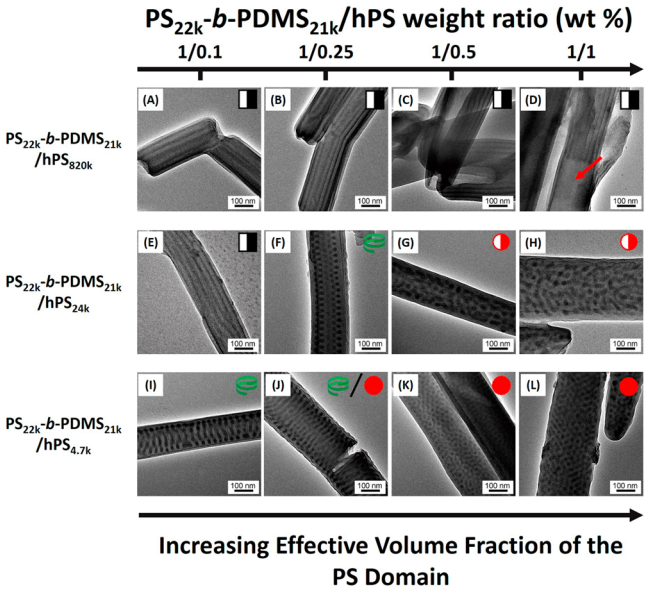


**Figure 5.** TEM images and corresponding symbols of $PS_{22k}$-*b*-$PDMS_{21k}$/hPS blend nanostructures with different weight ratios and hPS molecular weights: (A–D) $PS_{22k}$-*b*-$PDMS_{21k}$/$hPS_{820k}$, (E–H) $PS_{22k}$-*b*-$PDMS_{21k}$/$hPS_{24k}$, and (I–L) $PS_{22k}$-*b*-$PDMS_{21k}$/$hPS_{4.7k}$.

as described before, the morphologies change from concentric lamellar morphology, to multihelical morphology, and finally to spherical-like morphology as the weight ratio of $hPS_{24k}$ increases. For $PS_{22k}$-*b*-$PDMS_{21k}$/$hPS_{4.7k}$ ($r_M < 1$), as the blending ratio increases, the morphologies of $PS_{22k}$-*b*-$PDMS_{21k}$/$hPS_{4.7k}$ nanorods transform from multihelical morphology, to the intermediate state between multihelical morphology and spherical morphology, and finally to spherical morphology, as displayed in Figure 5I–L. It can be observed that the morphology transitions of $PS_{22k}$-*b*-$PDMS_{21k}$/$hPS_{4.7k}$ occur faster than that of $PS_{22k}$-*b*-$PDMS_{21k}$/$hPS_{24k}$, implying that more homopolymers "wet" the PS segments of the block copolymers in the case of $PS_{22k}$-*b*-$PDMS_{21k}$/$hPS_{4.7k}$ than that of $PS_{22k}$-*b*-$PDMS_{21k}$/$hPS_{24k}$. The implication is also indicated by the TEM images of $PS_{22k}$-*b*-$PDMS_{21k}$/$hPS_{4.7k}$ at higher blending ratios (1/0.5 and 1/1), where the spherical structures are not distorted compared to those for $PS_{22k}$-*b*-$PDMS_{21k}$/$hPS_{24k}$, as shown in Figure 5K and 5L.

For $PS_{22k}$-*b*-$PDMS_{21k}$/$hPS_{820k}$ ($r_M \gg 1$) in Figure 5A–D, only concentric lamellar morphologies are observed, mainly due to the much larger molecular weights of $hPS_{820k}$. As studied by Hashimoto et al., when $r_M \gg 1$, macrophase separation between the block copolymer and homopolymer exists. As a result, the concentric lamellar morphologies are maintained, and macrophase-separated $hPS_{820k}$ domains can be observed in some of the TEM images (Figure 5D), where a $hPS_{820k}$ macrodomain is indicated by a red arrow. The morphologies of $PS_{22k}$-*b*-$PDMS_{21k}$/hPS blend nanostructures with different weight ratios and hPS molecular weights are also summarized in Figure 6.

The unusual morphologies of the $PS_{22k}$-*b*-$PDMS_{21k}$/$hPS_{24k}$ blend nanostructures can be further confirmed by selectively etching the PDMS domains using an HF solution, as shown in Figure 7. After the selective removal process, the darker PDMS

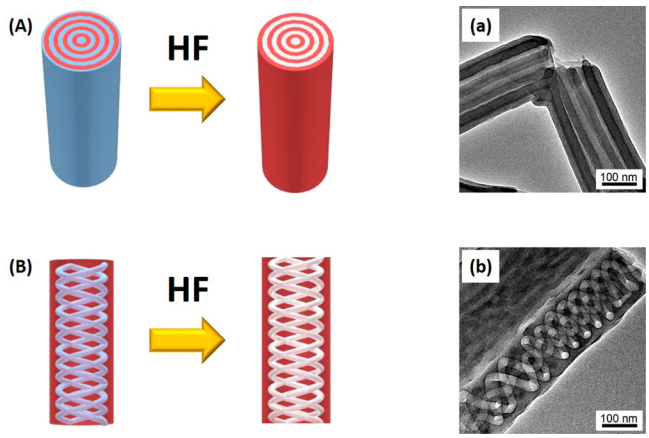


**Figure 7.** Graphical illustrations and corresponding TEM images for the $PS_{22k}$-*b*-$PDMS_{21k}$/$hPS_{24k}$ blend nanostructures with different weight ratios ($PS_{22k}$-*b*-$PDMS_{21k}$/$hPS_{24k}$) after the selective removal process: (A and a) 1/0 and (B and b) 1/0.25.

domains become lighter air domains in the TEM images. For the nanostructures with the concentric lamellar morphology, the concentric tubular PDMS domains can be selectively removed, and nanostructures containing tubular air channels can be obtained (Figure 7A and 7a). It is interesting to see that the concentric lamellar morphology is maintained after the selective removal process, which might be caused by the following two reasons. First, the PS and PDMS blocks in the

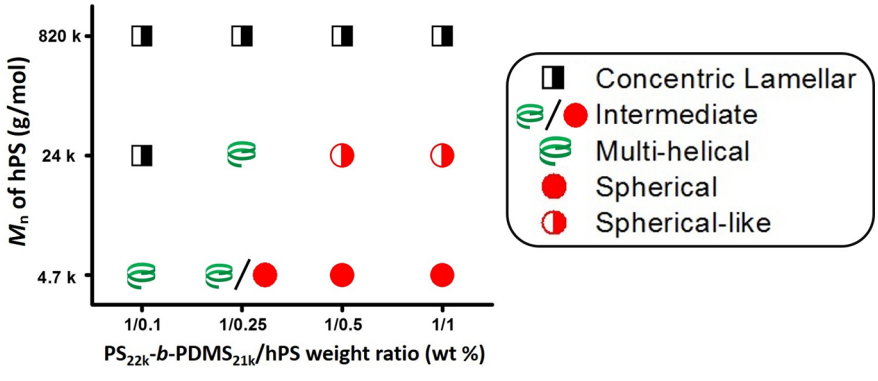


**Figure 6.** Morphology diagram of $PS_{22k}$-*b*-$PDMS_{21k}$/hPS blend nanostructures with different weight ratios and hPS molecular weights.


DOI: 10.1021/acsami.7b05415
ACS Appl. Mater. Interfaces 2017, 9, 21010–21016

nanopores might not align perfectly; therefore, some regions between the concentric lamellar domains are connected, holding the structures after the selective removal process. Second, some PDMS blocks may not be removed completely by the HF solution after the selective removal process; the residual PDMS domain can therefore sustain the concentric lamellar PS nanostructures. For the nanostructures with the multihelical morphology, the helical PDMS domains can be selectively removed, and nanostructures containing helical air channels can be obtained (Figure 7B and 7b). It has to be noted that the PDMS domains in the nanostructures with spherical-like morphology are difficult to be removed because the isolated PDMS domains are surrounded by the PS matrix.

In order to determine the rationality of the morphology transitions in our experimental results, simulation studies which investigated the morphologies of block copolymers confined in cylindrical nanopores are applied to compare with the experimental results obtained in this work. For the simulation studies, Shi et al. investigated the microphase separation of block copolymers with different intrinsic morphologies under the confinement effect of cylindrical nanopores with different degrees of confinement ($D/L_0$).[14] Zvelindovsky et al. also studied the microphase separation of block copolymers confined in cylindrical nanopores.[35] In addition, Zhang et al. investigated the block copolymer/homopolymer morphologies confined in cylindrical nanopores.[36] Morphologies similar to our experimental results, such as the multihelical morphologies, are obtained from these simulation works; the simulation parameters, however, are not identical to our experimental conditions because the block copolymer chains are introduced into the nanopores by solvent vapor-induced wetting in our works. Therefore, we believe that our research results should provide useful information on future simulation projects of block copolymers in confined geometries.

## CONCLUSION

In conclusion, we study the morphologies of $PS_{22k}$-*b*-$PDMS_{21k}$/hPS blend nanostructures confined in the nanopores of AAO templates using the SAINT method. The confined morphologies are observed to be controlled by the blending ratios between $PS_{22k}$-*b*-$PDMS_{21k}$ and hPS. Special morphologies, such as concentric lamellar morphology, multihelical morphology, and spherical-like morphology, can be obtained at different blending ratios. hPS with different molecular weights are also applied to investigate the effect of hPS on the morphologies of the $PS_{22k}$-*b*-$PDMS_{21k}$/hPS blend nanostructures. The PDMS domains can be selectively etched using the HF solution, and various porous PS nanostructures can be obtained. The selective removal process can not only further confirm the microphase separation of the $PS_{22k}$-*b*-$PDMS_{21k}$/$hPS_{24k}$ blend nanostructures but also generate porous PS nanostructures which can serve as scaffolds for refilling functional materials such as Au, Ag, and $TiO_2$.

## ASSOCIATED CONTENT

### Supporting Information

The Supporting Information is available free of charge on the ACS Publications website at DOI: 10.1021/acsami.7b05415.

TEM image and corresponding graphical illustrations showing the multihelical structures (PDF)

## AUTHOR INFORMATION


### Corresponding Author

*E-mail: jtchen@mail.nctu.edu.tw. Tel.: 886-3-5731631.

### ORCID

Jiun-Tai Chen: 0000-0002-0662-782X


### Notes

The authors declare no competing financial interest.

## ACKNOWLEDGMENTS

This work was supported by the Ministry of Science and Technology of the Republic of China. We thank Dr. U-Ser Jeng and Dr. Chun-Jen Su of the National Synchrotron Radiation Research Center (NSRRC) for their help in the SAXS experiments.

## REFERENCES


(1) Bates, F. S.; Fredrickson, G. H. Block Copolymer Thermodynamics - Theory and Experiment. *Annu. Rev. Phys. Chem.* **1990**, *41*, 525−557.

(2) Fasolka, M. J.; Mayes, A. M. Block Copolymer Thin Films: Physics and Applications. *Annu. Rev. Mater. Res.* **2001**, *31*, 323−355.

(3) Fredrickson, G. H.; Bates, F. S. Dynamics of Block Copolymers: Theory and Experiment. *Annu. Rev. Mater. Sci.* **1996**, *26*, 501−550.

(4) Park, C.; Yoon, J.; Thomas, E. L. Enabling Nanotechnology with Self Assembled Block Copolymer Patterns. *Polymer* **2003**, *44*, 6725−6760.

(5) Hawker, C. J.; Russell, T. P. Block Copolymer Lithography: Merging "Bottom-up" with "Top-Down" Processes. *MRS Bull.* **2005**, *30*, 952−966.

(6) Antonietti, M.; Wenz, E.; Bronstein, L.; Seregina, M. Synthesis and Characterization of Noble Metal Colloids in Block Copolymer Micelles. *Adv. Mater.* **1995**, *7*, 1000−1005.

(7) Kenausis, G. L.; Voros, J.; Elbert, D. L.; Huang, N. P.; Hofer, R.; Ruiz-Taylor, L.; Textor, M.; Hubbell, J. A.; Spencer, N. D. Poly(L-Lysine)-G-Poly(Ethylene Glycol) Layers on Metal Oxide Surfaces: Attachment Mechanism and Effects of Polymer Architecture on Resistance to Protein Adsorption. *J. Phys. Chem. B* **2000**, *104*, 3298−3309.

(8) Orilall, M. C.; Wiesner, U. Block Copolymer Based Composition and Morphology Control in Nanostructured Hybrid Materials for Energy Conversion and Storage: Solar Cells, Batteries, and Fuel Cells. *Chem. Soc. Rev.* **2011**, *40*, 520−535.

(9) Chen, J. T.; Hsu, C. S. Conjugated Polymer Nanostructures for Organic Solar Cell Applications. *Polym. Chem.* **2011**, *2*, 2707−2722.

(10) Park, M.; Harrison, C.; Chaikin, P. M.; Register, R. A.; Adamson, D. H. Block Copolymer Lithography: Periodic Arrays of Similar to 10(11) Holes in 1 Square Centimeter. *Science* **1997**, *276*, 1401−1404.

(11) Thurn-Albrecht, T.; Steiner, R.; DeRouchey, J.; Stafford, C. M.; Huang, E.; Bal, M.; Tuominen, M.; Hawker, C. J.; Russell, T. Nanoscopic Templates from Oriented Block Copolymer Films. *Adv. Mater.* **2000**, *12*, 787−791.

(12) Tseng, Y. T.; Tseng, W. H.; Lin, C. H.; Ho, R. M. Fabrication of Double-Length-Scale Patterns Via Lithography, Block Copolymer Templating, and Electrodeposition. *Adv. Mater.* **2007**, *19*, 3584−3588.

(13) Xiang, H. Q.; Shin, K.; Kim, T.; Moon, S. I.; McCarthy, T. J.; Russell, T. P. Block Copolymers under Cylindrical Confinement. *Macromolecules* **2004**, *37*, 5660−5664.

(14) Shi, A. C.; Li, B. H. Self-Assembly of Diblock Copolymers under Confinement. *Soft Matter* **2013**, *9*, 1398−1413.

(15) Stewart-Sloan, C. R.; Thomas, E. L. Interplay of Symmetries of Block Polymers and Confining Geometries. *Eur. Polym. J.* **2011**, *47*, 630−646.

(16) Dobriyal, P.; Xiang, H. Q.; Kazuyuki, M.; Chen, J. T.; Jinnai, H.; Russell, T. P. Cylindrically Confined Diblock Copolymers. *Macromolecules* **2009**, *42*, 9082−9088.




DOI: 10.1021/acsami.7b05415
*ACS Appl. Mater. Interfaces* 2017, 9, 21010−21016

(17) Masuda, H.; Fukuda, K. Ordered Metal Nanohole Arrays Made by a 2-Step Replication of Honeycomb Structures of Anodic Alumina. *Science* **1995**, *268*, 1466−1468.
(18) Lee, W.; Park, S. J. Porous Anodic Aluminum Oxide: Anodization and Templated Synthesis of Functional Nanostructures. *Chem. Rev.* **2014**, *114*, 7487−7556.
(19) Mijangos, C.; Hernandez, R.; Martin, J. A Review on the Progress of Polymer Nanostructures with Modulated Morphologies and Properties, Using Nanoporous Aao Templates. *Prog. Polym. Sci.* **2016**, *54*−*55*, 148−182.
(20) Cepak, V. M.; Martin, C. R. Preparation of Polymeric Micro- and Nanostructures Using a Template-Based Deposition Method. *Chem. Mater.* **1999**, *11*, 1363−1367.
(21) Chen, J. T.; Zhang, M. F.; Yang, L.; Collins, M.; Parks, J.; Avallone, A.; Russell, T. P. Templated Nanostructured Ps-B-Peo Nanotubes. *J. Polym. Sci., Part B: Polym. Phys.* **2007**, *45*, 2912−2917.
(22) Steinhart, M.; Wendorff, J. H.; Greiner, A.; Wehrspohn, R. B.; Nielsch, K.; Schilling, J.; Choi, J.; Gosele, U. Polymer Nanotubes by Wetting of Ordered Porous Templates. *Science* **2002**, *296*, 1997−1997.
(23) Steinhart, M.; Wehrspohn, R. B.; Gosele, U.; Wendorff, J. H. Nanotubes by Template Wetting: A Modular Assembly System. *Angew. Chem., Int. Ed.* **2004**, *43*, 1334−1344.
(24) Chang, C.-W.; Chi, M.-H.; Chu, C.-W.; Ko, H.-W.; Tu, Y.-H.; Tsai, C.-C.; Chen, J.-T. Microwave-Annealing-Induced Nanowetting: A Rapid and Facile Method for Fabrication of One-Dimensional Polymer Nanomaterials. *RSC Adv.* **2015**, *5*, 27443−27448.
(25) Chen, J. T.; Lee, C. W.; Chi, M. H.; Yao, I. C. Solvent-Annealing-Induced Nanowetting in Templates: Towards Tailored Polymer Nanostructures. *Macromol. Rapid Commun.* **2013**, *34*, 348−354.
(26) Chu, C. J.; Chung, P. Y.; Chi, M. H.; Kao, Y. H.; Chen, J. T. Three-Dimensional Block Copolymer Nanostructures by the Solvent-Annealing-Induced Wetting in Anodic Aluminum Oxide Templates. *Macromol. Rapid Commun.* **2014**, *35*, 1598−1605.
(27) Washburn, E. W. The Dynamics of Capillary Flow. *Phys. Rev.* **1921**, *17*, 273−283.
(28) Shin, K.; Xiang, H. Q.; Moon, S. I.; Kim, T.; McCarthy, T. J.; Russell, T. P. Curving and Frustrating Flatland. *Science* **2004**, *306*, 76.
(29) Sun, Y. M.; Steinhart, M.; Zschech, D.; Adhikari, R.; Michler, G. H.; Gosele, U. Diameter-Dependence of the Morphology of Ps-B-Pmma Nanorods Confined within Ordered Porous Alumina Templates. *Macromol. Rapid Commun.* **2005**, *26*, 369−375.
(30) Wang, Y.; Goesele, U.; Steinhart, M. Mesoporous Polymer Nanofibers by Infiltration of Block Copolymers with Sacrificial Domains into Porous Alumina. *Chem. Mater.* **2008**, *20*, 379−381.
(31) Xiang, H.; Shin, K.; Kim, T.; Moon, S. I.; McCarthy, T. J.; Russell, T. P. From Cylinders to Helices Upon Confinement. *Macromolecules* **2005**, *38*, 1055−1056.
(32) Cheng, M.-H.; Ko, H.-W.; Chung, P.-Y.; Chang, C.-W.; Chen, J.-T. Morphology Control of Three-Dimensional Nanostructures in Porous Templates Using Lamella-Forming Block Copolymers and Solvent Vapors. *Soft Matter* **2016**, *12*, 8087−8092.
(33) Tanaka, H.; Hasegawa, H.; Hashimoto, T. Ordered Structure in Mixtures of a Block Copolymer and Homopolymers. 1. Solubilization of Low Molecular Weight Homopolymers. *Macromolecules* **1991**, *24*, 240−251.
(34) Koizumi, S.; Hasegawa, H.; Hashimoto, T. Ordered Structure of Block Polymer/Homopolymer Mixtures, 4. Vesicle Formation and Macrophase Separation. *Makromol. Chem., Macromol. Symp.* **1992**, *62*, 75−91.
(35) Pinna, M.; Guo, X. H.; Zvelindovsky, A. V. Diblock Copolymers in a Cylindrical Pore. *J. Chem. Phys.* **2009**, *131*, 214902.
(36) Zhang, L. C.; Sun, M. N.; Pan, J. X.; Wang, B. F.; Zhang, J. J.; Wu, H. S. Copolymer-Homopolymer Mixtures in a Nanopore. *Chin. Phys. B* **2013**, *22*, 096401.


DOI: 10.1021/acsami.7b05415
*ACS Appl. Mater. Interfaces* 2017, 9, 21010−21016